Since January 2020 Elsevier has created a COVID-19 resource centre with free information in English and Mandarin on the novel coronavirus COVID-19. The COVID-19 resource centre is hosted on Elsevier Connect, the company's public news and information website.

Sensors & Actuators: B. Chemical 329 (2021) 129196

Contents lists available at ScienceDirect

Sensors and Actuators: B. Chemical

journal homepage: www.elsevier.com/locate/snb

Development of a SERS-based lateral flow immunoassay for rapid and ultra-sensitive detection of anti-SARS-CoV-2 IgM/IgG in clinical samples

Haifeng Liu [a,b,d,1], Erhei Dai [c,1], Rui Xiao [b,1], Zihui Zhou [a,b,d], Minli Zhang [b], Zikun Bai [b], Ying Shao [a,d], Kezong Qi [a,d], Jian Tu [a,d,*], Chongwen Wang [a,b,*], Shengqi Wang [b,*]

[a] Anhui Agricultural University, Hefei 230036, PR China
[b] Beijing Institute of Radiation Medicine, Beijing 100850, PR China
[c] Division of Liver Diseases, The Fifth Hospital of Shijiazhuang, Hebei Medical University, Shijiazhuang 050021, PR China
[d] Anhui Province Key Laboratory of Veterinary Pathobiology and Disease Control, Hefei 230036, PR China

ARTICLE INFO

Keywords:
SERS-LFIA
COVID-19
SARS-CoV-2
anti-SARS-CoV-2 IgM/IgG
Simultaneous detection

ABSTRACT

The accurate and rapid screening of serum antibodies against severe acute respiratory syndrome coronavirus 2 (SARS-CoV-2) is the key to control the spread of 2019 coronavirus disease (COVID-19). In this study, we reported a surface-enhanced Raman scattering-based lateral flow immunoassay (SERS-LFIA) for the simultaneous detection of anti-SARS-CoV-2 IgM/IgG with high sensitivity. Novel SERS tags labeled with dual layers of Raman dye were fabricated by coating a complete Ag shell on SiO_2 core (SiO_2@Ag) and exhibited excellent SERS signals, good monodispersity, and high stability. Anti-human IgM and IgG were immobilized onto the two test lines of the strip to capture the formed SiO_2@Ag-spike (S) protein-anti-SARS-CoV-2 IgM/IgG immunocomplexes. The SERS signal intensities of the IgM and IgG test zones were easily recorded by a portable Raman instrument and used for the high-sensitivity analysis of target IgM and IgG. The limit of detection of SERS-LFIA was 800 times higher than that of standard Au nanoparticle-based LFIA for target IgM and IgG. The SERS-LFIA biosensor was tested on 19 positive serum samples from COVID-19 patients and 49 negative serum samples from healthy people to demonstrate the clinical feasibility of our proposed assay. The results revealed that the proposed method exhibited high accuracy and specificity for patients with SARS-CoV-2 infection.

1. Introduction

The continued spread of severe acute respiratory syndrome coronavirus 2 (SARS-CoV-2), which is the specific pathogen of the 2019 coronavirus disease (COVID-19), has become a serious global public health concern [1,2]. The virus is highly contagious and can spread easily through the air (aerosols, respiratory droplets) and direct contact with body surfaces; thus, the virus has caused a high basic reproductive number ($R_0 > 3.7$) [3]. As of 21 July 2020, more than 14.5 million confirmed cases and more than 607 thousand deaths worldwide have been recorded by the World Health Organization [4]. Moreover, some patients with COVID-19 are asymptomatic but still infectious. No vaccines and medicines are available to prevent or treat COVID-19; therefore, the timely and accurate diagnosis of suspected cases is the most effective way to contain the outbreak. Some commonly used diagnostic techniques, including real-time reverse transcription-polymerase chain reaction (RT-PCR) and computed tomography imaging, have been applied for the clinical diagnosis of COVID-19 and exhibit good accuracy and reliability for severe cases [5–7]. However, these methods have some shortcomings in the rapid screening of early-stage patients and asymptomatic carriers because of their high false-negative rates, and these methods require long test time, specific testing place, professional personnel, and expensive equipment.

The serological testing of IgM and IgG against SARS-CoV-2 is an effective supplement to current clinical methods for COVID-19 diagnosis. According to the latest researches, anti-SARS-CoV-2 IgM/IgG can be observed in 31.8 %–40.9 % patients at 0–5 days after symptom onset by using enzyme-linked immunosorbent assay (ELISA) [8], and 94 % and 100 % of patients tested positive for virus-specific IgM and IgG, respectively, within 3 weeks after SARS-CoV-2 infection [9]. Moreover, the detectable periods of the two antibodies are remarkably different. IgM levels peak at 2–3 weeks after symptom onset and are reduced

* Corresponding authors.
E-mail addresses: tujian1980@126.com (J. Tu), wangchongwen1987@126.com (C. Wang), sqwang@bmi.ac.cn (S. Wang).
[1] The authors Haifeng Liu, Erhei Dai, and Rui Xiao contributed equally to this work.

https://doi.org/10.1016/j.snb.2020.129196
Received 23 July 2020; Received in revised form 4 November 2020; Accepted 7 November 2020
Available online 18 November 2020

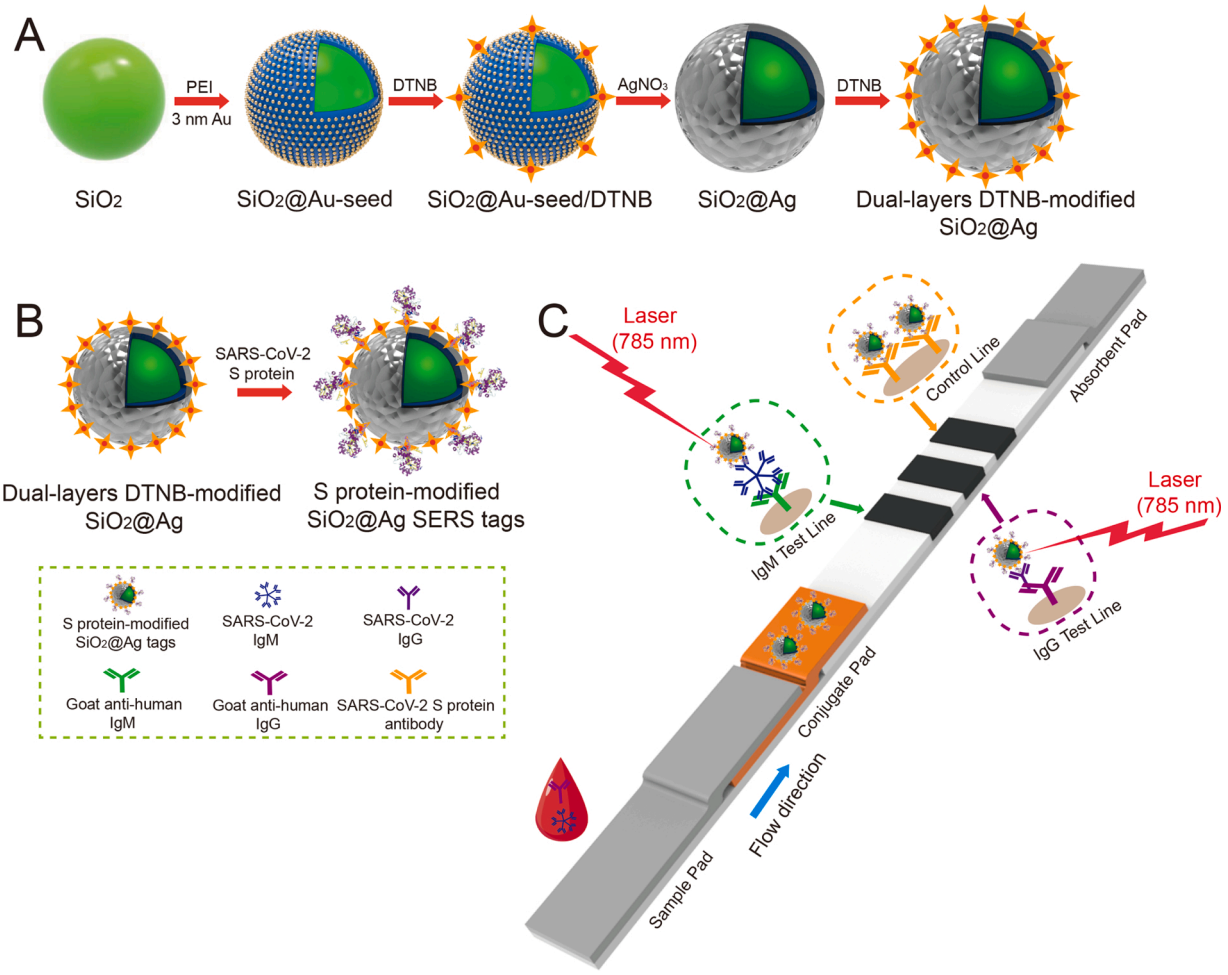

Scheme 1. (A) Schematic diagram of the preparation of the dual-layers DTNB-modified SiO_2@Ag NPs. (B) Preparation of SARS-CoV-2 S protein-modified SiO_2@Ag SERS tags. (C) Operating principle of the high-sensitivity and simultaneous analysis of anti-SARS-CoV-2 IgM/IgG via the SERS-LFIA strip.

rapidly in most patients, whereas the IgG titer peaks within 3 weeks and is maintained at high levels even over 2 months [10,11]. Thus, the combined detection of virus-specific IgM and IgG can help improve the detection rate and specificity for SARS-CoV-2-positive cases and assess the course and prognosis of the disease.

Lateral flow immunoassay (LFIA) has been considered one of the most popular point-of-care testing (POCT) techniques due to its simplicity, flexibility, speed, low cost, and wide adaptability [12–14]. The LFIA-based serological testing of anti-SARS-CoV-2 IgM/IgG is a good choice for the simple and effective diagnosis of COVID-19 because of the following advantages. (i) This test is suitable for plasma, serum, and whole blood to lessen the risk of exposure of healthcare workers to viral samples. (ii) It does not require professional personnel, and the operating space is not restricted by conditions. (iii) The test can be widely applied in any public places, such as schools, hospitals, customs, stations, and communities, to rapidly screen a large number of asymptomatic carriers. (iv) It can accurately distinguish COVID-19 from other respiratory viral infections, such as influenza, and gives results quickly. Several LFIA methods for COVID-19 diagnosis based on anti-SARS-CoV-2 IgM/IgG combined test have been reported [15–17]. However, these other methods were based on colorimetric analysis, which results in low sensitivity and poor quantitative ability. For example, a study by researchers at Guangzhou Medical University has reported that the sensitivity and specificity of the colloidal gold-based LFIA method with IgM and IgG simultaneous detection were only 88.66 % and 90.63 %, respectively [15]. We believe that increasing the sensitivity of the LFIA strip can effectively improve the detection rate of early-stage COVID-19 and reduce the corresponding rate of missed diagnoses.

In this study, we proposed a real-time two-channel surface-enhanced Raman scattering (SERS)-based LFIA biosensor to simultaneously detect anti-SARS-CoV-2 IgM/IgG with high sensitivity. SERS-LFIA strip is a new promising analytical technology that integrates functional SERS-encoded nanoparticles (NPs), also called SERS nanotags, into the LFIA system instead of the commonly used Au NPs as the signal reporter [18–20]. This technology can offer strong (high-sensitivity), specific (fingerprint feature), and stable (no photobleaching) SERS signals. More recently, several SERS-LFIA systems have been successfully developed for the sensitive and quantitative analysis of different target biomolecules, including heart disease biomarkers, tumor biomarkers, infection biomarkers, toxins, DNA markers, and respiratory viruses [21–26]. These researches revealed that the performance of the SERS-LFIA strip is highly dependent on the SERS activity and stability of SERS tags. Herein, we developed a novel SERS-LFIA biosensor for the high-sensitivity and simultaneous analysis of anti-SARS-CoV-2 IgM/IgG using dual-layers Raman molecule-loaded Ag-coated SiO_2 NPs (SiO_2@Ag NPs) as advanced SERS tags in clinical samples. This SiO_2@Ag SERS tag was composed of three parts: (i) a ~200 nm SiO_2 core as highly stable and monodispersed supporter, (ii) dual layers of Raman molecule 5,5-dithiobis-(2-nitrobenzoic acid) (DTNB) modified inside and outside the Ag shell to provide superior SERS signal, and (iii) a surface-modified SARS-CoV-2 spike (S) protein that specifically binds to anti-SARS-CoV-2 IgM/IgG. S protein-conjugated SiO_2@Ag SERS tags were used to prepare the conjugate pad, and anti-human IgM and IgG

were immobilized onto the two test zones to achieve the accurate detection of COVID-19. Thus, the combined analysis of anti-SARS-CoV-2 IgM/IgG was easily achieved by recording SERS signals of the corresponding test lines. The analytical ability and potential of the proposed SERS-LFIA for the simultaneous detection of anti-SARS-CoV-2 IgM/IgG were verified by testing 68 clinical serum specimens, which consisted of 19 positive and 49 negative samples. The proposed SERS-LFIA provides an efficient supplementary means for the accurate and rapid screening of SARS-CoV-2 infections.

2. Experimental section

2.1. Materials and chemicals

Tetraethyl orthosilicate (TEOS), 2-(N-morpholino) ethanesulfonic (MES), polyethyleneimine (PEI, 25 K), polyvinylpyrrolidone (PVP, 40 K), Tween 20, N-hydroxysuccinimide (NHS), N-(3-dimethylaminopropyl)-N′-ethylcarbodiimide hydrochloride (EDC), 5,5-dithiobis-(2-nitrobenzoic acid) (DTNB), sodium borohydride ($NaBH_4$), trisodium citrate ($Na_3C_6H_5O_7$, TSC), goat anti-human IgM, goat anti-human IgG, goat anti-rabbit IgG, bovine serum albumin (BSA) were obtained from Sigma-Aldrich (USA). SARS-CoV-2 S protein (recombinant) and S protein antibody (Ab) were obtained from Sino Biological Inc. (Beijing, China). Chloroauric acid tetrahydrate, sodium borohydride, formaldehyde (37 %, w/w), ammonia solution (28 %, w/w), chloroauric acid tetrahydrate ($HAuCl_4{\cdot}4H_2O$), and silver nitrate ($AgNO_3$) were obtained from Sinopharm Chemical Reagent Co., Ltd. (Shanghai, China). PBS buffer (10 mM, pH 7.4) and fetal bovine serum (FBS) were obtained from Thermo Fisher (Shanghai, China). Nitrocellulose (NC) membrane was purchased from Sartorius (UniSart CN95 and CN140, Spain) and Millipore Corporation (HF135, USA), respectively. The sample pad, absorbent pad, conjugate pad, and PVC bottom plate were obtained from Jieyi Biotechnology Co (Shanghai, China). All chemicals were of analytical grade and were utilized as received unless mentioned otherwise.

2.2. Instruments

High-resolution transmission electron microscope (HRTEM) images and elemental mapping images of SERS nanotags were obtained from Philips Tecnai G2 F20 microscope equipped with a STEM unit (Holland). UV–vis spectra were obtained from Shimadzu 2600 spectrometer. Zeta potential data were recorded with a Malvern Nano-ZS90 ZetaSizer (UK). Raman spectra were obtained from a portable Raman system (B&W Tek, i-Raman Plus BWS465−785H spectrometer) with 785 nm laser excitation. The Raman system is equipped with a 20 × microscope objective. The spot size of the big laser beam is 105 μm. Deionized water was prepared by Millipore-Q with the resistivity of 18.2 MΩ.

2.3. Preparation of SiO_2 NPs and 3 nm Au NPs

The SiO_2 NPs (~200 nm) were prepared by using an improved Stöber method [27]. Briefly, 3 mL of deionized water and 2 mL of ammonia solution (28 %) were added into 50 mL of ethanol, and the mixture was vigorously stirred for 20 min. Next, 2 mL of TEOS was rapidly injected, and the reaction was maintained with strong stirring at room temperature for 4 h. The resulting SiO_2 NPs were resuspended in 10 mL of ethanol by centrifugation (4600 rcf, 6 min) three times.

The 3 nm Au NPs were prepared based on the sodium borohydride reduction method reported by Fang et al. [28]. In brief, 3.8 mL of 1 wt.% TSC and 4 mL of 1 wt.% $HAuCl_4$ were added into 400 mL of deionized water. Then, 12 mL of 0.1 M freshly prepared $NaBH_4$ was quickly injected into the solution. The mixture was then stirred at room temperature for 4 h, and the Au NPs with an average particle size of 3 nm were obtained and stored at 4 °C.

2.4. Preparation of dual-layers DTNB-modified SiO_2@Ag NPs

The dual-layers DTNB-modified SiO_2@Ag NPs were fabricated in four successive steps as demonstrated in Scheme 1A. First, SiO_2@Au-seed NPs were prepared by the PEI-mediated absorption of 3 nm Au seed NPs onto the SiO_2 surface [29]. Briefly, 1 mL of the monodispersed SiO_2 NPs were put into 100 mL of deionized water, poured into the prepared PEI solution (10 mg/mL), and sonicated for 40 min to form SiO_2@PEI NPs. The resulting SiO_2@PEI NPs were rinsed two times with deionized water by centrifugation (3400 rcf, 6 min) and then added into 200 mL of 3 nm Au NP solution. After sonication for 30 min, the formed SiO_2@Au-seed NPs were separated by centrifugation (2400 rcf, 6 min) and stored in 10 mL of ethanol until the next use.

Second, the SiO_2@Au-seed NPs were sonically mixed with a freshly prepared DTNB-ethanol solution (10 μM) for 1 h to form SiO_2@Au-seed/DTNB NPs. Then, excess DTNB was removed by centrifugation (2400 rcf, 6 min) and resuspended in original volume with ethanol. Third, the SiO_2@Ag core-shell NPs were synthesized by employing a seed growth method through the reduction of $AgNO_3$ by formaldehyde. Briefly, 1 mL of SiO_2@Au-seed/DTNB NPs was added into 30 mL of deionized water with 1.5 wt.% polyvinylpyrrolidone and 0.35 mM $AgNO_3$. Then, 35 μL of formaldehyde solution (~37 %) and 70 μL of ammonia solution (~28 %) were successively added into the solution under vigorous sonication. After 5 min, the obtained SiO_2@Ag NPs were purified twice by centrifugation (850 rcf, 6 min) and then resuspended in 10 mL of ethanol.

Finally, the second layer of DTNB was modified on the surface of SiO_2@Ag NPs to fabricate dual-layers DTNB-loaded nanotags. In short, 10 mL of SiO_2@Ag NPs was mixed with a freshly prepared DTNB-ethanol solution (10 μM), and the mixture was vigorously sonicated for 1 h. The synthesized dual-layers DTNB-modified SiO_2@Ag NPs were separated by centrifugation (850 rcf, 6 min) and stored in 10 mL of ethanol.

2.5. SARS-CoV-2 S protein immobilized on the SiO_2@Ag SERS tags

The dual-layers DTNB-modified SiO_2@Ag NPs were conjugated with SARS-CoV-2 S protein by amide reaction as demonstrated in Scheme 1B. In brief, 500 μL of dual-layers DTNB-modified SiO_2@Ag solution was centrifuged and redispersed in 500 μL of MES buffer (100 mM, pH 5.5). Then, 50 μL of 10 mM EDC and 10 μL of 100 mM NHS were added, and the mixture was sonicated for 15 min. The mixture was then centrifuged to remove excess activator, resuspended in 500 μL of 10 mM PBS solution (pH7.4), and incubated with S protein (30 μg/mL) for 2 h at room temperature under shaking. The unreacted carboxyl groups of SiO_2@Ag SERS tags were blocked with 80 μL of 10 % BSA for 1 h. Finally, the resulting S protein-modified SiO_2@Ag SERS tags were rinsed with 10 mM PBST (containing 0.05 % Tween 20, pH7.4), resuspended with 500 μL of 10 mM PBS solution containing 0.05 % Tween 20, 5% BSA, 0.02 % NaN_3. The prepared SERS tags were evenly dropped in the conjugate pad and freeze-dried in a vacuum.

2.6. Preparation of two-channel SERS-LFIA for anti-SARS-CoV-2 IgM/IgG simultaneous detection

The SERS-LFIA biosensor consists of an absorption pad, an NC membrane, a conjugate pad, and a sample pad as demonstrated in Scheme 1C. Each component was installed on a plastic adhesive backing plate in sequence. The two test lines were separately sprayed onto 0.5 mg/mL of anti-human IgM and 0.6 mg/mL anti-human IgG, whereas the control line was coated onto 0.5 mg/mL of S protein antibody. All three lines were spaced approximately 5 mm apart on the NC membrane via a line dispensing instrument (BioDot XYZ3000). The fabricated NC membrane was dried at 37 °C for 1 h. Finally, the assembled test strips were cut into 3.5 mm width using a programmable cutter (Zeta Corporation, South Korea) for future use.

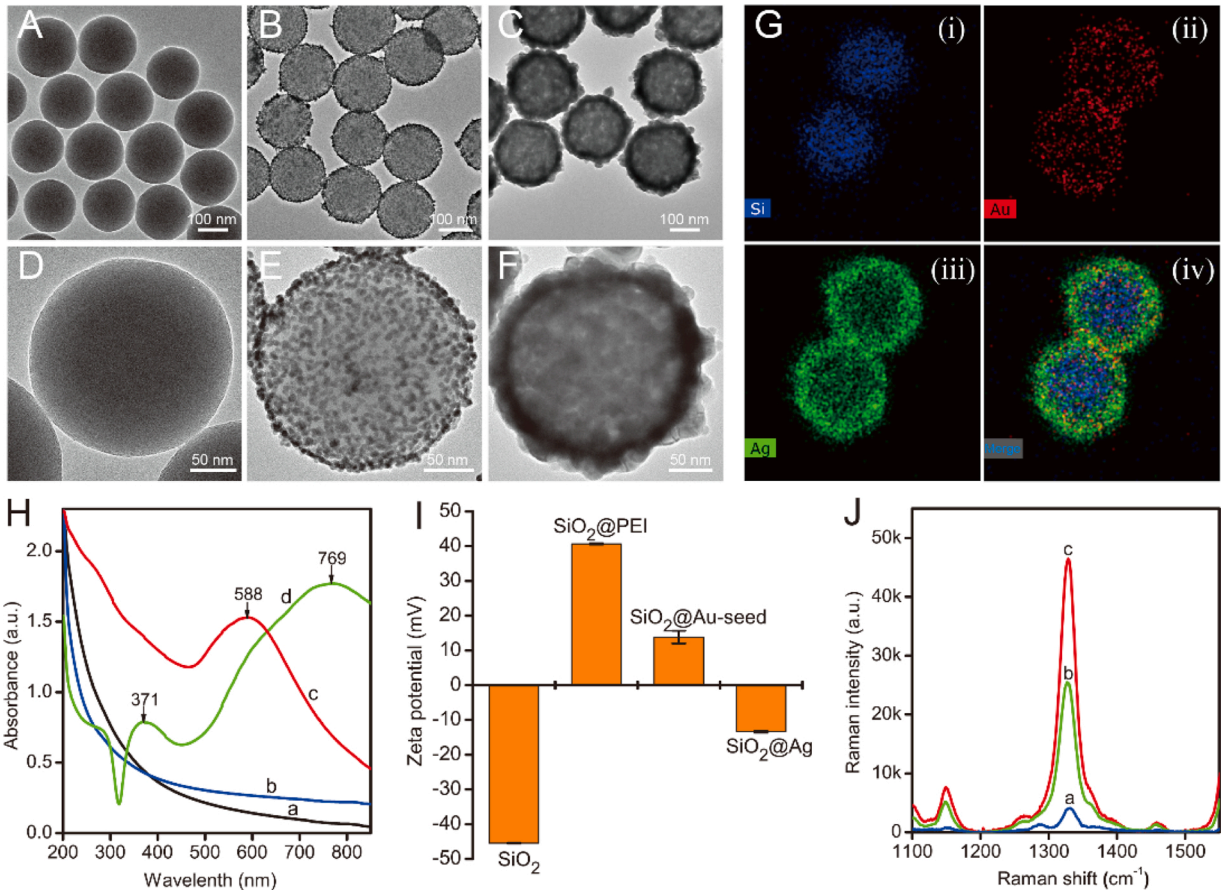

Fig. 1. HRTEM images of the prepared (A) SiO_2 NPs, (B) SiO_2@Au-seed NPs, and (C) SiO_2@Ag NPs with their corresponding enlarged images in (D), (E), and (F), respectively. (G) Element mapping results of the SiO_2@Ag NPs. UV–vis spectra (H) and zeta potentials (I) of the as-synthesized products from each stage. (J) SERS intensities of (a) SiO_2@Au-seed/DTNB NPs, (b) SiO_2@Ag/DTNB NPs, and (c) dual-layers DTNB-modified SiO_2@Ag NPs.

2.7. Clinical sample test via two-channel SERS-LFIA

19 COVID-19 positive sera and 49 COVID-19 negative sera were collected from the Fifth Hospital of Shijiazhuang. The patients whose sera collected were diagnosed by RT-PCR. The study was conducted under the Declaration of Helsinki, and it is evaluated and approved by the Ethics Committee of the hospital with the case number of 2020−001. The clinical serum samples were diluted to various folds and tested by two-channel SERS-LFIA to assess the effectiveness of the presented approach. SERS measurement was performed with a power of 10 mW for 1 s by using 785 nm excitation. The obtained data were recorded for the high-sensitivity analysis of COVID-19. The receiver operating characteristic (ROC) curve was used to assess the diagnostic ability of the method for COVID-19 at low antibody concentrations. The predicted probability of IgM and IgG co-diagnosis was calculated for each dilution according to binary logistic regression equations; then, the ROC curves of IgM, IgG, and IgM/IgG were plotted; and the area under the ROC curve (AUC) were calculated. Operations on the ROC curve were conducted in SPSS 19.0.

3. Results and discussion

3.1. Principle of SERS-based LFIA for the simultaneous detection of anti-SARS-CoV-2 IgM/IgG

Scheme 1C illustrates the testing principle of the SERS-based LFIA for the simultaneous detection of anti-SARS-CoV-2 IgM/IgG in human serum based on typical antibody-antigen reactions. SARS-CoV-2 S protein was labeled with dual-layers DTNB-modified SiO_2@Ag NPs, which served as advanced SERS nanotags and can bind to anti-SARS-CoV-2 IgM/IgG specifically. Two test lines and one control line were built on the LFIA strip. Anti-human IgM, anti-human IgG, and anti-S protein antibody were dispensed on the first test line (IgM line), second test line (IgG line), and control line (C line), respectively. The clinical sample containing virus-specific IgM and IgG antibodies was mixed with the running buffer and subsequently dropped on the sample pad to operate the LFIA test. The solution migrates along the strip toward the absorbent pad under capillary forces. Specific IgM and IgG were captured by the S protein-modified SiO_2@Ag SERS tags as the solution gets through the conjugated pad to form SiO_2@Ag-S protein-IgM/IgG immunocomplexes. The formed complexes were captured by the IgM and IgG lines as the solution continued to flow, and excess SERS tags were then captured by the anti-S protein antibody on the C line. If the sample has no target anti-SARS-CoV-2 IgM/IgG, then immunocomplex cannot be formed and no SERS tags will be captured by the test lines. Based on this principle, the presence of anti-SARS-CoV-2 IgM/IgG with different concentrations can be simultaneously analyzed by measuring the SERS signal intensities on the corresponding test zones.

3.2. Characterization of the S protein-modified SiO_2@Ag nanotags

The key features of SERS-LFIA, including its high sensitivity, high stability, and good repeatability, rely on the performance of SERS tags. In this study, novel SiO_2@Ag SERS tags were designed and acted as ideal SERS tags with monodispersity, good stability, and excellent SERS activity. As illustrated in Scheme 1A, the SiO_2@Ag SERS tags were synthesized by attaching two layers of DTNB molecules in and on the Ag shells of SiO_2@Ag NPs based on our previously proposed PEI-mediated

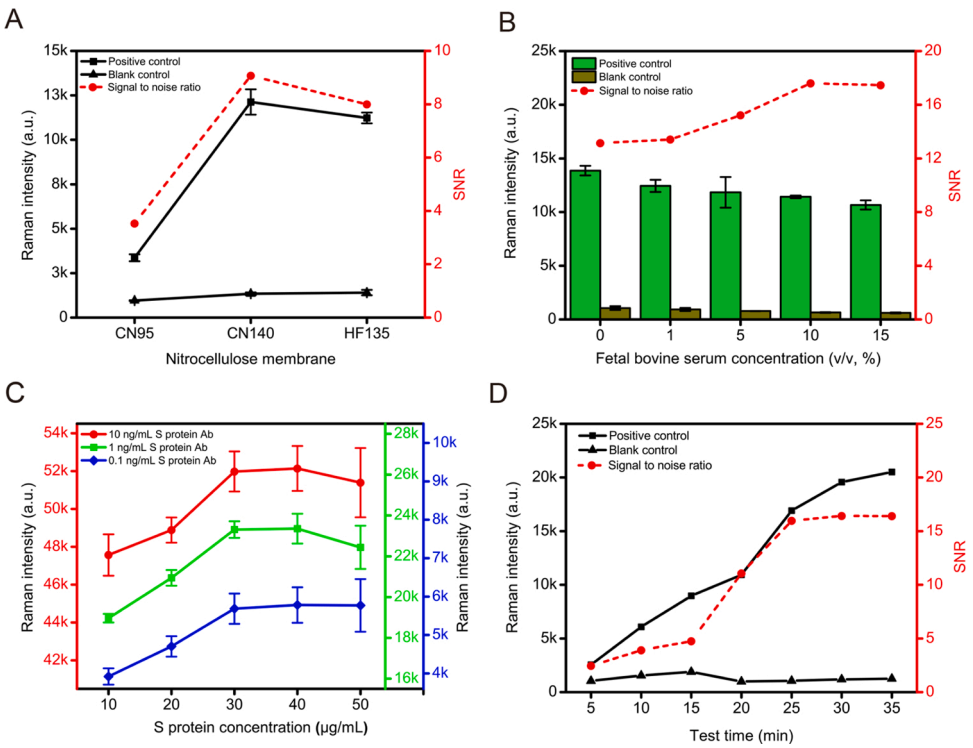

Fig. 2. Optimization of (A) NC membrane, (B) running solution, (C) S protein amount for the preparation of immuno-SiO_2@Ag SERS tags, and (D) immunoreaction time for the SERS-LFIA system. 1 ng/mL of S protein antibody was used as a positive sample, and PBS containing 1% Tween 20 was used as a blank control.

seed growth strategy [30,31]. We first synthesized monodispersed SiO_2 NPs as the stable core for SERS tags. The HRTEM image in Fig. 1A shows that uniform SiO_2 NPs with an average size of 210 nm were fabricated via the Stöber method. Many 3 nm Au NPs were adsorbed on the surface of SiO_2@PEI NPs by electrostatic adsorption after PEI coating. Fig. 1B clearly shows the formed SiO_2@Au-seed NPs with densely adsorbed Au seeds on their surface, which possess abundant sites for DTNB modification and Ag shell growth. The first layer of DTNB was easily labeled on the Au seeds of SiO_2@Au-seed NPs by forming Au-S chemical bond. As described in our previous work, the outer Ag shell can be well coated on the SiO_2 core by the reduction of Ag^+ on the Au seeds. Fig. 1C displays the HRTEM image of the as-prepared SiO_2@Ag NPs with an average particle size of 240 nm. Figs. 1D–F shows the magnified HRTEM images of SiO_2 NPs, SiO_2@Au-seed NPs, and SiO_2@Ag NPs, respectively. These HRTEM images confirmed that a complete and rough Ag shell was coated successfully on the surface of SiO_2 NPs. The elemental composition of SiO_2@Ag NPs was characterized by energy-dispersive X-ray (EDX) spectroscopy (Fig. S1) and element mapping analysis (Fig. 1G). Four elements, namely, Si, O, Au, and Ag, were found in the SiO_2@Ag NPs, but the Cu signal came from the copper grid. Moreover, the element mapping results clearly showed the typical core-shell structure of the SiO_2@Ag NPs. From an optical point of view, the UV–vis spectrum of SiO_2@Ag NPs was remarkably changed after Ag shell formation (Fig. 1H). The absorption peak of SiO_2@Au-seed NPs was centered at 588 nm (curve c in Fig. 1H), whereas no obvious absorption peak of SiO_2 NPs and SiO_2@PEI NPs were observed (curves a and b in Fig. 1H). The SiO_2@Ag NPs displayed transversal and longitudinal plasmon resonances at 371 and 769 nm (curve d in Fig. 1H), respectively, from the Ag shell coating. The absorption peak at 371 nm corresponds to the Ag shell, whereas the longitudinal localized surface plasmon resonance (LSPR) band refers to the strong surface plasmonic coupling of the core-shell nanostructure. Notably, the LSPR band of SiO_2@Ag NPs at 769 nm nearly provided a 785 nm excitation wavelength, which can greatly improve the SERS activity of nanotags. The zeta potentials of SiO_2 NPs, SiO_2@PEI NPs, SiO_2@Au-seed NPs, and SiO_2@Ag NPs were –45.49, +40.66, +13.82, and –13.42 mV, respectively (Fig. 1I), which indicated the strong positive charge of the PEI layer and the negative charge of the Ag shell. The original zeta potentials data are shown in Fig. S2. The regular and stable changes in potential during reactions indicate that the fabrication process of SiO_2@Ag NPs is dependable. In this study, Raman molecule DTNB was chosen to build the SERS tags because of its strong characteristic Raman peaks and terminal carboxyl groups, which can be directly used for protein conjugation. The dual layers of DTNB molecules were integrated into SERS tags to generate stronger SERS signals. The SERS activities of SiO_2@Au-seed/DTNB NPs, SiO_2@Ag/DTNB NPs, and dual-layers DTNB-modified SiO_2@Ag NPs were investigated by comparing the intensity of the main SERS peak of DTNB at 1328 cm^{-1}. As displayed in Fig. 1J, the SERS intensity of the dual-layers DTNB-modified SiO_2@Ag NPs is nearly twice that of SiO_2@Ag/DTNB NPs and beyond eleven times that of SiO_2@Au--seed/DTNB NPs. These results confirmed the superior SERS activity of our proposed dual-layers DTNB-modified SiO_2@Ag NPs, which is critical to the subsequent SERS-LFIA.

3.3. Optimization and evaluation of the SERS-LFIA system

A general model for human serum antibody detection was first established to optimize the SiO_2@Ag-based SERS-LFIA. Commercial SARS-CoV-2 S protein antibody (rabbit monoclonal antibody) was used to simulate anti-SARS-CoV-2 IgM/IgG in patients with COVID-19, which can also be specifically detected by S protein-modified SiO_2@Ag SERS tags. Goat anti-rabbit IgG (1 mg/mL) was sprayed onto the CN140 membrane as the test line. This model can be used for the quantitative analysis of the anti-S protein antibody in serum samples. Many studies proved that choosing the proper NC membrane and running solution can generate the best assay sensitivity [19,21,32]. These two parameters of the LFIA strip have an obvious impact on the flow rate of SERS tags and the immune binding reaction between SERS tags-S protein-target IgM/IgG and the test lines. The effects of three types of NC membrane, namely, CN95, CN140, and HF135, were first investigated considering

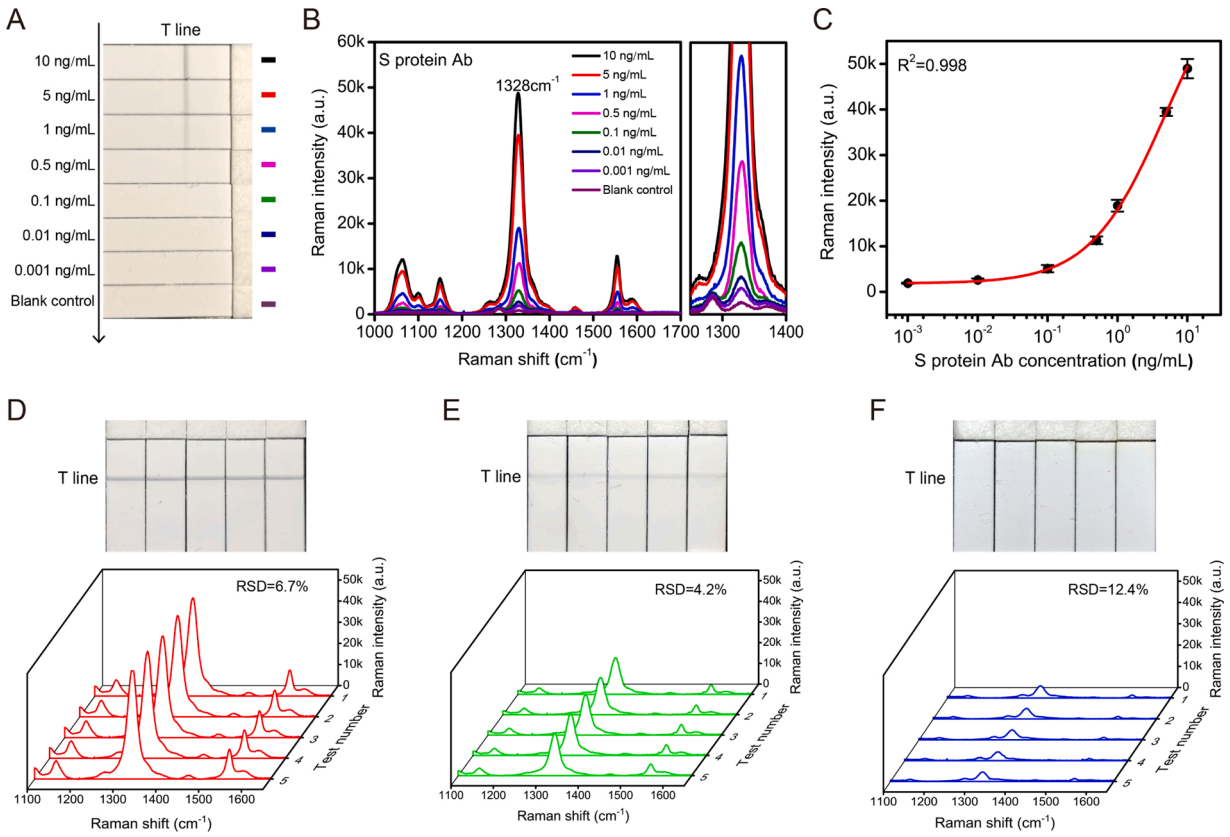

Fig. 3. (A) Images of SERS-LFIA strips with a single T line after application of different S protein antibody concentrations (10–0.001 ng/mL). (B) Raman spectra measured in the corresponding test lines and the enlarged viewport at the 1328 cm^{-1} characteristic peak. (C) Calibration curve of SiO_2@Ag SERS-based LFIA for S protein antibody. Image and Raman spectra of five tests of S protein antibody at concentrations of (D) 10, (E) 1, and (F) 0.1 ng/mL.

the big size of SiO_2@Ag SERS tags. As shown in Fig. 2A, the CN140 membrane (~10 μm pore size)-based LFIA strip can lead to optimal signal-to-noise ratio (SNR) for target S protein antibody detection. Thus, we selected CN140 as the reaction platform to build the SERS-LFIA system. Given our previous work, PBST solution (10 mM, pH 7.4, 1% Tween 20) was used to prepare the running solution because of its good biocompatibility and fluidity for immuno-SiO_2@Ag SERS tags [33,34]. Herein, fetal bovine serum (FBS) was added to the PBST solution to inhibit the nonspecific adsorption of the NC membrane. The highest SNR on the test line was achieved when the concentration of FBS was increased to 10 % (Fig. 2B). Next, the optimum amount of S protein-coupled SiO_2@Ag SERS tags was investigated. Activated dual-layers DTNB-modified SiO_2@Ag solution (0.5 mL) was first incubated with different concentrations (10–50 μg/mL) of S protein. Then, the as-obtained SiO_2@Ag-S protein was dispensed onto the glass fiber paper to prepare the conjugate pad. The constructed SERS-LFIA strips were used to test three spiked samples with high (10 ng/mL), medium (1 ng/mL), and low (0.1 ng/mL) concentrations of SARS-CoV-2 S protein antibody. As shown in Fig. 2C, the SERS intensity on the T line of SERS-LFIA increased with increasing S protein concentration (10–30 μg/mL) and no longer increased at 40–50 μg/mL of S protein. These results indicated that 30 μg of S protein per 1 mL of SERS tags is the optimal labeling amount, at which the saturated SERS signal on the T lines was observed. As revealed by Fig. 2D, the increase in incubation time (0–35 min) generated a higher SERS signal intensity on the test line. However, an incubation time longer than 25 min did not cause a better SNR in the test zone; thus, 25 min of immunoreaction time was suitable for the proposed SERS-LFIA.

It should be noted that the sensitivity and reliability of the SERS-LFIA are highly dependent on the performance of SiO_2@Ag SERS tags. Three kinds of SiO_2@Ag tags with different SiO_2 core (~88 nm, 210 nm, and 420 nm) were fabricated and tested (Supporting Information S1 and Fig. S3(A–F)). As revealed in Fig. S3G, 240 nm SiO_2@Ag tags-based SERS-LFIA strip was found to provide the highest SNR on the test line for the detection of 1 ng/mL of S protein antibody. Thus, 240 nm SiO_2@Ag tags were chosen in this work to achieve a highly sensitive analysis of target IgM/IgG on the SERS-LFIA strip.

The analytical performance of SiO_2@Ag SERS-based LFIA, including detection sensitivity, quantitative ability, and reproducibility, was assessed after major parameter optimization. The solution containing the SARS-CoV-2 S protein antibody was diluted in a range of 10–0.001 ng/mL and then tested under the established protocol. Fig. 3A displays the photographs of SiO_2@Ag-LFIA testing different concentrations of S protein antibody (10–0.001 ng/mL). Fewer SERS tag-S protein antibody complexes were formed as the S protein antibody concentration decreased; thus, fewer immune complexes were caught on the test line. Dark black bands on the test lines could be observed by the naked eye at concentrations above 1 ng/mL (Fig. 3A). Quantitative analysis was conducted by recording the SERS intensities of the captured SiO_2@Ag SERS tags on the T zones. The SERS spectra with different concentrations of S protein antibody are recorded in Fig. 3B. The Raman intensities weakened with decreasing S protein concentration. Its main peak (1328 cm^{-1}) can be still distinguished from that of the blank control in the enlarged viewport even at concentrations as low as 1 pg/mL. The corresponding calibration curve was plotted by S protein antibody concentration and is shown in Fig. 3C. The limit of detection (LOD) of the SERS results was 1 pg/mL, which was calculated via the IUPAC standard method ($LOD = Y_{blank} + 3SD$, where Y_{blank} represents the average SERS signal of the blank control and 3SD represent three times the standard deviation of the blank control) [35,36]. By comparison, the LOD of the SERS-LFIA strips based on the SERS signal was 1000 times more sensitive than that obtained from the SiO_2@Ag aggregation-based

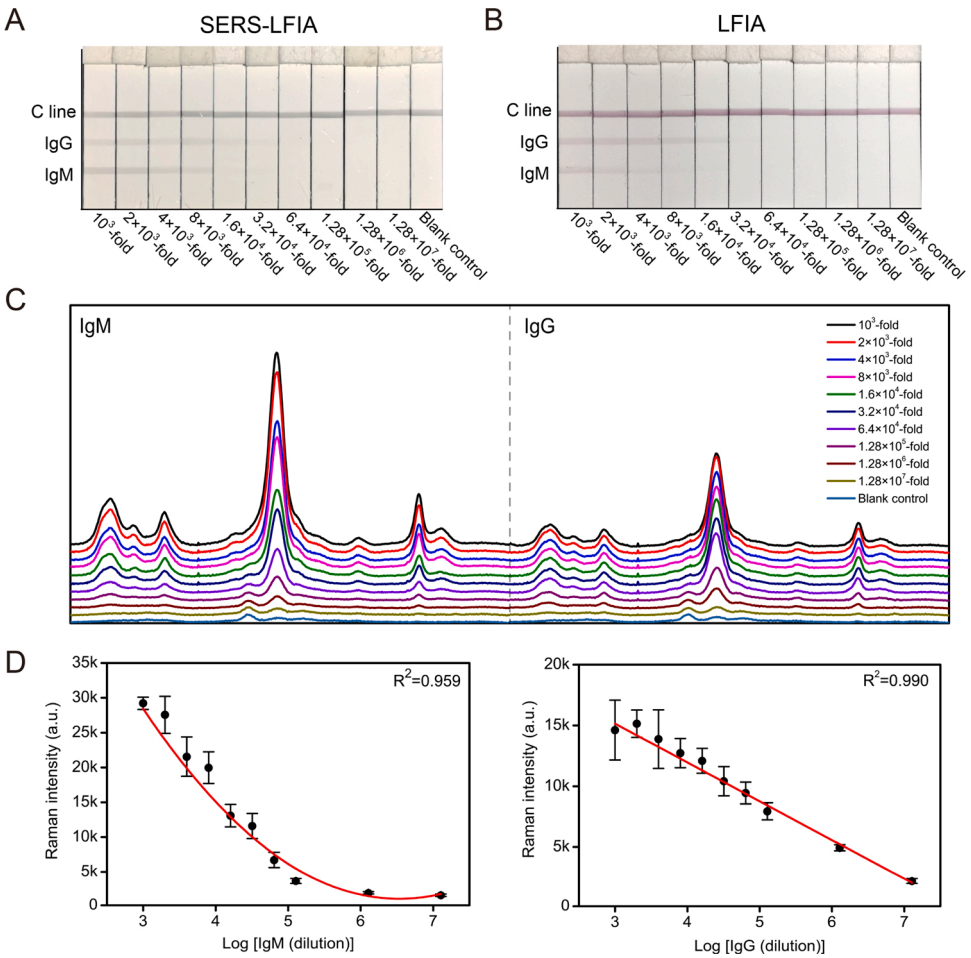

Fig. 4. Images of (A) SiO_2@Ag-based SERS-LFIA strips and (B) Au NP-based LFIA strips for anti-SARS-CoV-2 IgM/IgG detection at different dilutions. (C) SERS spectra measured from the corresponding test lines of IgM and IgG. (D) Calibration curves with SERS signal at 1328 cm^{-1} for target IgM (left) and IgG (right).

visualization result. The high sensitivity of the proposed SERS-LFIA can be attributed to the great SERS enhancement provided by SiO_2@Ag SERS tags. Five different batches of SERS-LFIA strips were prepared and used to detect the different concentrations of S protein antibody (10, 1, and 0.1 ng/mL) to evaluate the repeatability of the method. As shown in Figs. 3D–F, the SERS intensities of the test lines for each batch are similar. The relative standard deviation values of five independent testing for 10, 1, and 0.1 ng/mL of S protein antibody were calculated to be 6.7 %, 4.2 %, and 12.4 %, respectively, which suggest that the method was highly reproducible. Moreover, the long-term stability of SiO_2@Ag-based SERS-LFIA was investigated. The detection performance of SERS-LFIA was not obviously weakened after 60 days of storage (Fig. S4). All these results indicated that the proposed SERS-LFIA can serve as a highly sensitive detection tool for specific antibodies.

3.4. Analytical performance of the proposed SERS-LFIA for clinical serum samples

A clinical serum from a patient with COVID-19 was tested by the SiO_2@Ag-based SERS-LFIA to directly assess the feasibility of the proposed method for the detection of anti-SARS-CoV-2 IgM/IgG. The clinical serum was confirmed IgM and IgG positive for SARS-CoV-2 by commercial colloid gold strip kit as shown in Fig. S5. The positive serum specimen was first serially diluted from 10^3-fold to 1.28×10^7-fold by an optimized working solution and then added to the sample of SERS-LFIA strips. As shown in Fig. S6, an obvious hook effect was observed in low-dilution groups (10–10^2-fold dilution), which caused false-negative results due to the excessive unlabeled antigen occupied by the captured antibodies on the test line. The visualization results of the two test lines above the 10^3-fold dilutions were inversely proportional to the dilution of the positive serum as displayed in Fig. 4A. The dark color on the IgM and IgG lines were decreased gradually with increasing dilution (10^3–1.6×10^4 fold), and the dark band was difficult to identify with the naked eye in the test lines for IgM and IgG at concentrations lower than 1.6×10^4-fold dilution. All the tested strips displayed a distinct dark band on the control zone, which indicates that the SERS-LFIA was working properly. Fig. 4C illustrates the average SERS spectra of the 20 measurements for the IgM (left) and IgG lines (right) for the various dilutions (10^3–1.28×10^7-fold) of the confirmed positive serum. It was still visible with the Raman spectra at lower concentrations (up to 1.28×10^7-fold dilution) when the limit of colorimetric analysis was reached (1.6×10^4-fold dilution). This result indicated that a small amount of SiO_2@Ag-S protein-IgM/IgG immunocomplexes immobilized on the test lines, even invisible to the human eye, can generate enough SERS intensities for target detection. Moreover, the SERS intensities of the IgM and IgG lines concomitantly decreased with the decreasing concentrations of target anti-SARS-CoV-2 IgM/IgG in the sample. The calibration curves were plotted from the logarithm of the established dilutions and the SERS intensities of corresponding IgM and IgG lines for quantitative analysis as shown in Fig. 4D. The SERS signals of the test lines for anti-SARS-CoV-2 IgM/IgG display wide dynamic relationships with the concentrations of the two viral-specific antibodies with $R^2 = 0.959$ for anti-SARS-CoV-2 IgM and $R^2 = 0.990$ for anti-SARS-CoV-2 IgG. The LOD values for anti-SARS-CoV-2 IgM/IgG were estimated to be 1.28×10^7-fold dilution by the IUPAC standard method, which is 800 times lower than that of the visualization results.

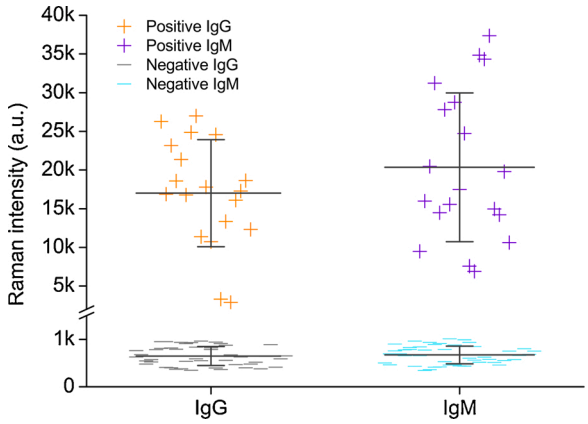

Fig. 5. SERS intensities scatter plot of anti-SARS-CoV-2 IgM and IgG for 68 serum samples, including 19 positive sera and 49 normal sera.

Moreover, a standard Au NP-based LFIA strip was established by using the S protein-modified Au NPs to directly compare the sensitivity of the proposed SERS-LFIA (Fig. 4B). By comparison, the visual detection ability of the standard Au NP-based strip was equivalent to that of the proposed SERS-LFIA. Thus, the overall sensitivity of SERS-LFIA based on SiO_2@Ag SERS tags was 800 times that of standard Au NP-based LFIA for the simultaneous analysis of anti-SARS-CoV-2 IgM/IgG. Besides, the SiO_2@Ag-based SERS-LFIA for anti-SARS-CoV-2 IgM/IgG simultaneous detection also showed a wide dynamic range, which covered seven orders of magnitude. In addition, the detection performance of the proposed SERS-LFIA strips for whole blood samples was evaluated (Fig. S7). The results indicated that SiO_2@Ag-based SERS-LFIA can work well in blood samples. Therefore, all these results demonstrate that the proposed SERS-LFIA possesses high sensitivity, stability, and wide detection range and can be employed as a sensitive POCT method for the clinical diagnosis of COVID-19.

We further tested 49 normal serum samples from healthy donors and 19 positive serum samples that were collected from confirmed patients with COVID-19 to assess the clinical potential of the proposed SERS-LFIA. The serum samples were diluted with running buffer (10^3-fold), and then 90 μL of diluted samples were used to operate the SERS-LFIA. The SERS signal results on the IgM and IgG test zones were collected after 25 min of reaction. As shown in Fig. S8A, most of the positive samples exhibited distinct dark IgM and IgG lines, except the IgG lines of samples P10 and P12. No test line was observed in the negative group in Fig. S8B. The SERS signal intensities at 1328 cm^{-1} on the IgM and IgG lines of all the tested LFIA strips were measured under the SERS mode and are displayed in Fig. 5. All the IgM and IgG lines of the positive samples, including the test lines invisible to the naked eye (the IgG lines of P10 and P12), generated strong SERS signals with minimum intensity values that are greater than 2881. The SERS signal intensities on the test zones of the 49 negative samples were rather low (<1014). According to the SERS results of the T-tests between the positive and negative groups, the signal of the positive samples was greatly higher than that of the negative group ($P < 0.01$, Fig. S9). Based on the IUPAC method (the

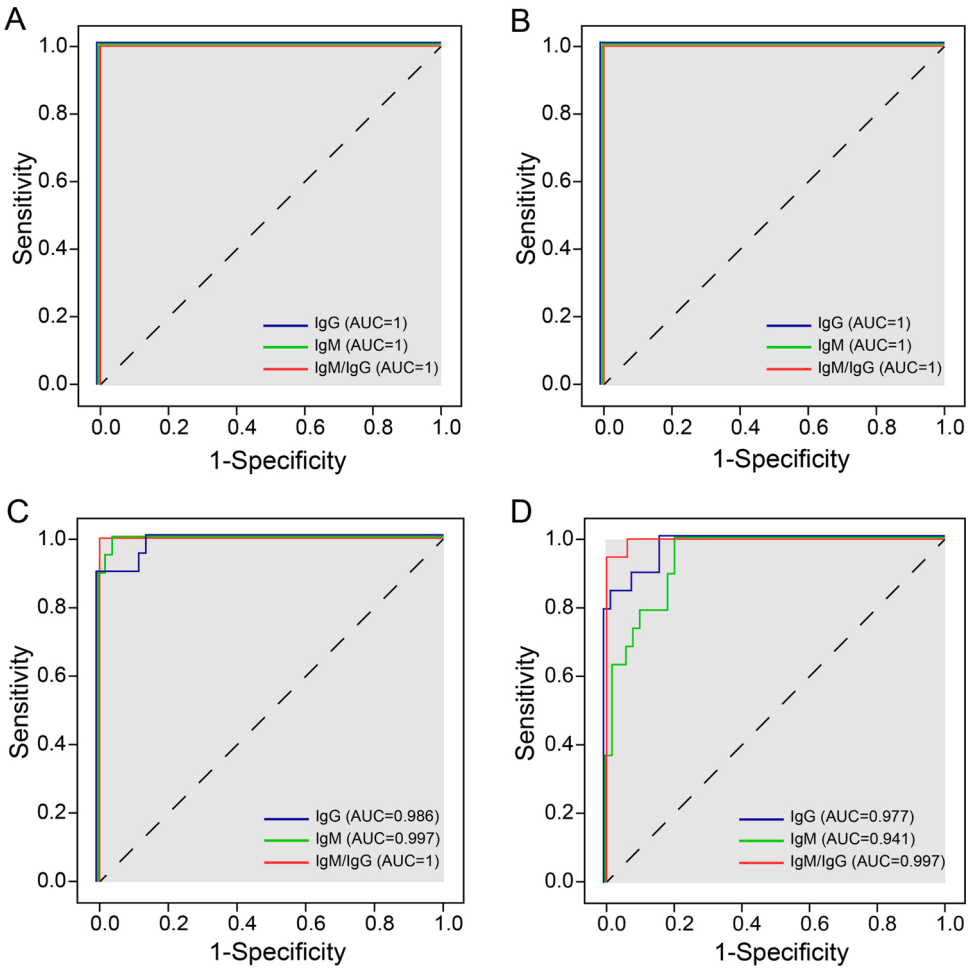

Fig. 6. ROC curve analysis of the diagnostic value of SERS-LFIA to detect COVID-19 positive sera (n = 19) from the negative sera (n = 49) at different dilutions: (A) 10^3-fold, (B) 10^4-fold, (C) 10^5-fold, and (D) 10^6-fold dilutions.

mean of negative sera + 3SD), the cutoff value was calculated as 1249. Therefore, the IgM and IgG lines of the serum samples with SERS intensities higher than 1249 were considered anti-SARS-CoV-2 IgM/IgG positive, whereas those with intensities lower than 1249 were defined as anti-SARS-CoV-2 IgM/IgG negative. All these results indicated the high specificity and sensitivity of our proposed method toward COVID-19 positive sera.

Furthermore, ROC curves were used to evaluate the diagnostic value of the SERS-LFIA. The SERS signal intensities from the IgM and IgG zones of the tested LFIA-strips were used to analyze. The ROC curve analysis results are displayed in Table S1 and Fig. 6, which reflect the diagnostic ability of the SERS-LFIA at different serum dilutions. The ROC curves resulted in the AUC value of 1 for IgM and IgG for the diagnosis of serum samples with 10^3–10^4-fold dilution (Fig. 6A and B). The combination of IgM and IgG had an excellent AUC value (1–0.997) for higher dilution groups (10^5–10^6-fold) compared with IgM (0.997–0.941) and IgG alone (0.986–0.977) (Fig. 6C and D). These results revealed the higher accuracy and specificity of the proposed SERS-LFIA based on IgM and IgG simultaneous detection than individual IgM or IgG antibody test, especially for the positive serum specimen with a low concentration of anti-SARS-CoV-2 IgM/IgG. Notably, several recent studies have shown that the concentration of SARS-CoV-2 specific IgM in the serum of patients with COVID-19 decreased sharply and even disappeared within 1 month after disease onset, whereas the high concentration of virus-specific IgG titer was maintained for more than 2 months in infected persons [9,11]. Thus, the proposed SERS-LFIA has the great potential to detect the trace amounts of virus-specific IgM and IgG in serum samples at the early stage and also provides critical information to determine the course of SARS-CoV-2 infection. We believe our method can greatly facilitate the timely and accurate detection of SARS-CoV-2 infection on-site.

4. Conclusion

In summary, a rapid and ultra-sensitive SERS-LFIA biosensor was proposed for the simultaneous detection of anti-SARS-CoV-2 IgM/IgG in clinical samples. A novel dual-layers DTNB-modified SiO_2@Ag SERS tag was introduced in the LFIA system to act as a strong and stable signal reporter. Meanwhile, SARS-CoV-2 S protein was modified onto the SiO_2@Ag surface to bind to target virus-specific antibodies to ensure the feasibility and specificity of the biosensor. Anti-human IgM and IgG antibodies were immobilized on the two test lines of the NC membrane to ensure the simultaneous capture and detection of anti-SARS-CoV-2 IgM/IgG in one test. Analysis of the SERS signal intensities of corresponding test zones of the LFIA strip revealed that the detection sensitivity of the proposed method for virus-specific IgM and IgG was 800 times more sensitive than that of the standard Au-based LFIA method. The clinical application potential of the SERS-LFIA was further validated using 68 clinical serum samples, including 19 positive serum samples and 49 negative serum samples. The results revealed the 100 % accuracy and specificity of the SERS-LFIA for the combined analysis of IgM and IgG. Considering its high sensitivity, accuracy, and specificity, the proposed method may be used for the rapid screening of COVID-19 during early infection, when the levels of target IgM and IgG antibodies are still low and difficult to detect by detection methods, such as Au NP-based LFIA strip, indirect immunofluorescence assay, and ELISA.

CRediT authorship contribution statement

Haifeng Liu: Methodology, Writing - original draft. **Erhei Dai:** Methodology, Writing - original draft. **Rui Xiao:** Methodology, Data curation. **Zihui Zhou:** Methodology. **Minli Zhang:** Methodology. **Zikun Bai:** Methodology. **Ying Shao:** Methodology. **Kezong Qi:** Supervision, Funding acquisition. **Jian Tu:** Supervision, Data curation. **Chongwen Wang:** Conceptualization, Writing - original draft, Writing - review & editing, Supervision. **Shengqi Wang:** Funding acquisition, Writing - review & editing, Supervision.

Declaration of Competing Interest

The authors declare no conflict of interest.

Acknowledgements

This study was supported by the National Natural Science Foundation of China (Grant no. 81830101), the Natural Science Foundation of Anhui Province (Grant no. 1908085QB85), and the National S&T Major Project for Infectious Diseases Control (Grant nos. 2018ZX10712001-010, 2018ZX10101003-001).

Appendix B. Supplementary data

Supplementary material related to this article can be found, in the online version, at doi:https://doi.org/10.1016/j.snb.2020.129196.

References

[1] F. Zhou, T. Yu, R. Du, G. Fan, Y. Liu, Z. Liu, et al., Clinical course and risk factors for mortality of adult inpatients with COVID-19 in Wuhan, China: a retrospective cohort study, Lancet 395 (2020) 1054–1062.
[2] V. Coronaviridae Study Group of the International Committee on Taxonomy of, The species Severe acute respiratory syndrome-related coronavirus: classifying 2019-nCoV and naming it SARS-CoV-2, Nat. Microbiol. 5 (2020) 536–544.
[3] W.J. Guan, Z.Y. Ni, Y. Hu, W.H. Liang, C.Q. Ou, J.X. He, et al., Clinical Characteristics of Coronavirus Disease 2019 in China, New England J. Med. Surg. Collat. Branches Sci. 382 (2020) 1708–1720.
[4] (COVID-19): Situation Report – 183, WHO. Coronavirus Disease, 2019. https://www.who.int/docs/default-source/wha-70-and-phe/20200721-covid-19-sitrep-183.pdf?sfvrsn=b3869b3_2.
[5] R. Wölfel, V.M. Corman, W. Guggemos, M. Seilmaier, S. Zange, M.A. Müller, et al., Virological assessment of hospitalized patients with COVID-2019, Nature 581 (2020) 465–469.
[6] Y. Pan, D. Zhang, P. Yang, L.L.M. Poon, Q. Wang, Viral load of SARS-CoV-2 in clinical samples, Lancet Infect. Dis. 20 (2020) 411–412.
[7] F. Cui, H.S. Zhou, Diagnostic methods and potential portable biosensors for coronavirus disease 2019, Biosens. Bioelectron. 165 (2020), 112349.
[8] W. Liu, L. Liu, G. Kou, Y. Zheng, Y. Ding, W. Ni, et al., Evaluation of Nucleocapsid and Spike protein-based enzyme-linked immunosorbent assays for detecting antibodies against SARS-CoV-2, J. Clin. Microbiol. 58 (2020) e00461–20.
[9] Q.X. Long, B.Z. Liu, H.J. Deng, G.C. Wu, K. Deng, Y.K. Chen, et al., Antibody responses to SARS-CoV-2 in patients with COVID-19, Nat. Med. (2020) 1–4.
[10] H. Hou, T. Wang, B. Zhang, Y. Luo, L. Mao, F. Wang, et al., Detection of IgM and IgG antibodies in patients with coronavirus disease 2019, Clin Transl Immunol 9 (2020), e01136.
[11] X. Xu, J. Sun, S. Nie, H. Li, Y. Kong, M. Liang, et al., Seroprevalence of immunoglobulin M and G antibodies against SARS-CoV-2 in China, Nat. Med. (2020) 1–3.
[12] M. Tian, L. Lei, W. Xie, Q. Yang, C.M. Li, Y. Liu, Copper deposition-induced efficient signal amplification for ultrasensitive lateral flow immunoassay, Sensor Actuat B-Chem 282 (2019) 96–103.
[13] J.D. Bishop, H.V. Hsieh, D.J. Gasperino, B.H. Weigl, Sensitivity enhancement in lateral flow assays: a systems perspective, Lab Chip 19 (2019) 2486–2499.
[14] P. Brangel, A. Sobarzo, C. Parolo, B.S. Miller, P.D. Howes, S. Gelkop, et al., A serological point-of-Care test for the detection of IgG antibodies against ebola virus in human survivors, ACS Nano 12 (2018) 63–73.
[15] Z. Li, Y. Yi, X. Luo, N. Xiong, Y. Liu, S. Li, et al., Development and clinical application of a rapid IgM-IgG combined antibody test for SARS-CoV-2 infection diagnosis, J. Med. Virol. (2020) 1–7.
[16] Z. Chen, Z. Zhang, X. Zhai, Y. Li, L. Lin, H. Zhao, et al., Rapid and sensitive detection of anti-SARS-CoV-2 IgG, using lanthanide-doped nanoparticles-based lateral flow immunoassay, Anal. Chem. 92 (2020) 7226–7231.
[17] H. Li, Z. Liu, Y. He, Y. Qi, J. Chen, Y. Ma, et al., A new and rapid approach for detecting COVID-19 based on S1 protein fragments, Clin. Transl. Med. (2020) 1–6.
[18] S.H. Lee, J. Hwang, K. Kim, J. Jeon, S. Lee, J. Ko, et al., Quantitative serodiagnosis of scrub typhus using surface-enhanced raman scattering-based lateral flow assay platforms, Anal. Chem. 91 (2019) 12275–12282.
[19] L. Blanco-Covian, V. Montes-Garcia, A. Girard, M.T. Fernandez-Abedul, J. Perez-Juste, I. Pastoriza-Santos, et al., Au@Ag SERRS tags coupled to a lateral flow immunoassay for the sensitive detection of pneumolysin, Nanoscale 9 (2017) 2051–2058.
[20] B.N. Khlebtsov, D.N. Bratashov, N.A. Byzova, B.B. Dzantiev, N.G. Khlebtsov, SERS-based lateral flow immunoassay of troponin I by using gap-enhanced Raman tags, Nano Res. 12 (2018) 413–420.
[21] X. Wang, N. Choi, Z. Cheng, J. Ko, L. Chen, J. Choo, Simultaneous detection of dual nucleic acids using a SERS-Based lateral flow assay biosensor, Anal. Chem. 89 (2017) 1163–1169.

[22] D. Zhang, L. Huang, B. Liu, H. Ni, L. Sun, E. Su, et al., Quantitative and ultrasensitive detection of multiplex cardiac biomarkers in lateral flow assay with core-shell SERS nanotags, Biosens. Bioelectron. 106 (2018) 204–211.
[23] D. Zhang, L. Huang, B. Liu, E. Su, H.-Y. Chen, Z. Gu, et al., Quantitative detection of multiplex cardiac biomarkers with encoded SERS nanotags on a single T line in lateral flow assay, Sensor Actuat B-Chem 277 (2018) 502–509.
[24] J. Hwang, S. Lee, J. Choo, Application of a SERS-based lateral flow immunoassay strip for the rapid and sensitive detection of staphylococcal enterotoxin B, Nanoscale 8 (2016) 11418–11425.
[25] C. Wang, C. Wang, X. Wang, K. Wang, Y. Zhu, Z. Rong, et al., Magnetic SERS strip for sensitive and simultaneous detection of respiratory viruses, ACS Appl Mater Inter 11 (2019) 19495–19505.
[26] X. Liu, X. Yang, K. Li, H. Liu, R. Xiao, W. Wang, et al., Fe3O4@Au SERS tags-based lateral flow assay for simultaneous detection of serum amyloid A and C-reactive protein in unprocessed blood sample, Sensor Actuat B-Chem 320 (2020), 128350.
[27] T. Liu, D. Li, D. Yang, M. Jiang, An improved seed-mediated growth method to coat complete silver shells onto silica spheres for surface-enhanced Raman scattering, Colloids Surf. A Physicochem. Eng. Asp. 387 (2011) 17–22.
[28] Y. Fang, S. Guo, C. Zhu, Y. Zhai, E. Wang, Self-assembly of cationic polyelectrolyte-functionalized graphene nanosheets and gold nanoparticles: a two-dimensional heterostructure for hydrogen peroxide sensing, Langmuir 26 (2010) 11277–11282.
[29] C. Wang, M. Li, Q. Li, K. Zhang, C. Wang, R. Xiao, et al., Polyethyleneimine-mediated seed growth approach for synthesis of silver-shell silica-core nanocomposites and their application as a versatile SERS platform, RSC Adv. 7 (2017) 13138–13148.
[30] C. Wang, J. Xu, J. Wang, Z. Rong, P. Li, R. Xiao, et al., Polyethylenimine-interlayered silver-shell magnetic-core microspheres as multifunctional SERS substrates, J. Mater. Chem. C Mater. Opt. Electron. Devices 3 (2015) 8684–8693.
[31] C. Wang, P. Li, J. Wang, Z. Rong, Y. Pang, J. Xu, et al., Polyethylenimine-interlayered core-shell-satellite 3D magnetic microspheres as versatile SERS substrates, Nanoscale 7 (2015) 18694–18707.
[32] W. Shen, C. Wang, X. Yang, C. Wang, Z. Zhou, X. Liu, et al., Synthesis of raspberry-like nanogapped Fe3O4@Au nanocomposites for SERS-based lateral flow detection of multiple tumor biomarkers, J. Mater. Chem. C Mater. Opt. Electron. Devices 8 (37) (2020) 12854–12864.
[33] C. Wang, R. Xiao, S. Wang, X. Yang, Z. Bai, X. Li, et al., Magnetic quantum dot based lateral flow assay biosensor for multiplex and sensitive detection of protein toxins in food samples, Biosens. Bioelectron. 146 (2019) 111754.
[34] C. Wang, W. Shen, Z. Rong, X. Liu, B. Gu, R. Xiao, et al., Layer-by-layer assembly of magnetic-core dual quantum dot-shell nanocomposites for fluorescence lateral flow detection of bacteria, Nanoscale 12 (2019) 795–807.
[35] J. Hu, Y.Z. Jiang, L.L. Wu, Z. Wu, Y. Bi, G. Wong, et al., Dual-signal readout nanospheres for rapid point-of-Care detection of ebola virus glycoprotein, Anal. Chem. 89 (2017) 13105–13111.
[36] X. Fu, Z. Cheng, J. Yu, P. Choo, L. Chen, J. Choo, A SERS-based lateral flow assay biosensor for highly sensitive detection of HIV-1 DNA, Biosens. Bioelectron. 78 (2016) 530–537.

Haifeng Liu is a master student under the guidance of Dr. Jian Tu at Anhui Agricultural University in China. His work focuses on the development of SERS-based biosensors.

Erhei Dai is a chief physician in the Fifth Hospital of Shijiazhuang, Hebei province, China. His research interests include the development of diagnostic methods for virus and bacterial pathogens, development of the prognosis model of virus-related liver disease.

Rui Xiao is currently an associate professor at the Beijing Institute of Radiation Medicine. Her research interests include SERS-based biosensors and SERS materials fabrication.

Zihui Zhou is a master student under the guidance of Dr. Chongwen Wang at Anhui Agricultural University in China. Her research interests include the development of surface-enhanced Raman scattering (SERS)-based lateral flow immunoassay biosensor and nanomaterials-based sensors.

Minli Zhang is a technical director at the Beijing Institute of Radiation Medicine in China. Her work focuses on the development of nanoparticle-based biosensors.

Ying Shao is a technicist in Anhui Agricultural University in China. Her work focuses on the development of SERS-based biosensors.

Kezong Qi is currently a professor at Anhui Agricultural University. His research interests include the nanoparticle-based detection method.

Jian Tu is currently an associate professor at Anhui Agricultural University in China. His work focuses on the development of nanoparticle-based detection methods.

Chongwen Wang received his pH.D. in biomedical engineering from Beijing University of Technology in 2018. He is currently an associate professor at Anhui Agricultural University in China. His work focuses on the preparation and application of novel metal and magnetic nanomaterials.

Shengqi Wang is currently a professor at the Beijing Institute of Radiation Medicine. His research interests include DNA/protein biosensing, virology, and pharmacology.